Journal of Hazardous Materials 316 (2016) 204–213

Contents lists available at ScienceDirect

Journal of Hazardous Materials

journal homepage: www.elsevier.com/locate/jhazmat

The spatial distribution patterns of condensed phase post-blast explosive residues formed during detonation

Nadia Abdul-Karim[a,*], Christopher S. Blackman[a], Philip P. Gill[b], Kersti Karu[a]

[a] Department of Chemistry, University College London, WC1H 0AJ London, UK
[b] Centre for Defence Chemistry, Cranfield University, Shrivenham SN6 8LA, UK

HIGHLIGHTS

- Particle distribution patterns from explosive releases are analyte specific.
- Applications of mathematical models to particle movement are unsuitable.
- The dominant particle dispersal mechanism is the smoke plume, governed by the wind.

ARTICLE INFO

Article history:
Received 14 January 2016
Received in revised form 15 April 2016
Accepted 28 April 2016
Available online 6 May 2016

Keywords:
Explosive
Detonation
Particle
Dispersal
Residue

ABSTRACT

The continued usage of explosive devices, as well as the ever growing threat of 'dirty' bombs necessitates a comprehensive understanding of particle dispersal during detonation events in order to develop effectual methods for targeting explosive and/or additive remediation efforts. Herein, the distribution of explosive analytes from controlled detonations of aluminised ammonium nitrate and an RDX-based explosive composition were established by systematically sampling sites positioned around each firing. This is the first experimental study to produce evidence that the post-blast residue mass can distribute according to an approximate inverse-square law model, while also demonstrating for the first time that distribution trends can vary depending on individual analytes. Furthermore, by incorporating blast-wave overpressure measurements, high-speed imaging for fireball volume recordings, and monitoring of environmental conditions, it was determined that the principle factor affecting all analyte dispersals was the wind direction, with other factors affecting specific analytes to varying degrees. The dispersal *mechanism* for explosive residue is primarily the smoke cloud, a finding which in itself has wider impacts on the environment and fundamental detonation theory.

1. Introduction

The majority of research related to post-blast chemical data is centred on the development of novel sampling techniques and optimisation of analytical methods for trace explosive residues. Whilst these are necessary and important research foci, a distinctly disproportionate amount of research has been conducted in establishing the types of trace chemicals that may remain following detonation in the first instance. For example, how do explosive residues remain in their undecomposed form during detonation, how do they disperse, and therefore where can they be found in the environment? By answering such questions, we would be better placed to act in the aftermath of a radiological dispersive device ('dirty' bomb) or improvised explosive device modified to contain chemical or biological warfare agents, for example. Knowledge regarding the dispersal and fate of particles would not only benefit environmental decontamination efforts but would also assist in forensic investigations. Undetonated explosive particles that remain after detonation can provide critical intelligence regarding the explosive charge used and indicate the perpetrators of an explosive attack [1]. Current knowledge regarding post-blast residue location has developed with experience over time but the prevailing requirement to be prepared to face new threats [2], as well as validate and strengthen the scientific underpinning of forensic practices [3], calls for further research.

Given the impracticalities of experimenting with explosive charges modified with hazardous additives, we first focus on monitoring the distribution trends of known explosive ana-

* Corresponding author.
E-mail addresses: nadia.abdul-karim.10@ucl.ac.uk (N. Abdul-Karim), c.blackman@ucl.ac.uk (C.S. Blackman), p.p.gill@cranfield.ac.uk (P.P. Gill), kersti.karu@ucl.ac.uk (K. Karu).

http://dx.doi.org/10.1016/j.jhazmat.2016.04.081

lytes during detonation. In doing so, it will become possible to develop models that can assist in elucidating the particle dispersal behaviours of other, more harmful, potential additives. Both 1,3,5-Trinitroperhydro-1,3,5-triazine (RDX) and ammonium nitrate (AN) are widely used explosives, in both military and criminal contexts, which leave undetonated residues and for which the decomposition mechanisms have been studied extensively. In the solid state, the most supported mechanism for the initial unimolecular decomposition step of RDX begins with the loss of a single NO_2 molecule [4] via homolytic cleavage of an N—NO_2 bond [5,6], which is followed by the rupture of the chain into intermediate products. The final gaseous products formed through these decompositions are energetically stable and form strongly bonded species such as CO_2, H_2O and N_2 [7] (Eq. (1)).

$$C_3H_6N_6O_{6(s)} \rightarrow 3CO_{(g)} + 3H_2O_{(g)} + 3N_{2(g)} \quad (1)$$

Whilst RDX has a deficient number of oxidising atoms for complete combustion (oxygen balance (OB) of −21.6%), theoretically, no parent explosive molecules should remain following detonation. The energy release is increased as the fuel-rich product gases undergo afterburning with atmospheric oxygen, which is facilitated by turbulent mixing within the fireball [8].

The decomposition of the bimolecular AN has been studied broadly but is not understood as well [9]. Investigations into the effect of the shock stimulus on AN decomposition have indicated the break-up of the NH_4^+ ion occurs initially, possibly followed by decomposition of the NO_3^- ion [10]. Ultimately, the gaseous products formed are N_2, H_2O and O_2 [7]. As a fuel-lean explosive (OB of +20%) AN combusts fully (Eq. (2)).

$$NH_4NO_{3(s)} \rightarrow N_{2(g)} + 2H_2O_{(g)} + \tfrac{1}{2}O_{2(g)} \quad (2)$$

The addition of combustible light metals (e.g. aluminium) to non-ideal explosives such as AN, improves their energetic efficiency by increasing the reaction velocity and temperature [7,11]. In the case of aluminised ammonium nitrate (AlAN), the high temperature AN decomposition products heat the aluminium particles, which evaporate upon reaching their ignition temperature and react in the gaseous phase; either aerobically with oxygen in shock compressed air or anaerobically with oxidants in the detonation products [12,13]. Reactions occur behind the principle reaction front during the expansion of the gases [13–16], with the main combustion product being aluminium oxide [14,15]. Given that the afterburning of aluminium releases more energy, which further enhances the blast effects by increasing the overpressure impulse produced [12,15,17], it is again counter-intuitive to expect any undecomposed AN molecules to remain post-blast.

Due to the transient, dynamic nature of detonation, it is an understandably challenging task to experimentally investigate the means by which undetonated explosive residue 'survives' detonation; it is generally accepted that incomplete combustion will always occur to varying degrees depending on the explosive type. It may be possible to infer the mechanism(s) however, by investigating how distribution trends vary between different explosives. Our recent review [18] of explosive residue dispersion theories highlighted the effects of the blast-wave and ambient wind field as the two principal potential mechanisms by which explosive residue is dispersed – neither of which have been tested experimentally. The residue distribution patterns have been purported to be based on an inverse-square law distribution [19] (Eq. (3)); a seemingly logical theory for spherical explosive charges (if the particles are assumed to be ejected uniformly from the charge surface), but one that has not been verified.

$$Mass_1/Mass_2 = Distance_2{}^2/Distance_1{}^2 \quad (3)$$

One of the factors thought to affect the resulting detectable amount of explosive residue is the fireball [19]; the exposure of which onto nearby surfaces may cause degradation of any deposited intact explosive particles and therefore alter any preliminary inverse-square type distributions.

Experimental work to date is mainly limited to studies [20,21] conducted to understand residue distribution at ground-level in order to control explosives leaching through soil and into groundwater. Fewer studies have investigated particle distribution by incorporating perpendicularly positioned sampling sites around detonations of both military and improvised explosives. The few that have [22–25] found conflicting trends of both decreasing and increasing amounts of explosive residue as a function of increasing distance from the charge centre, where issues with sample analysis may have affected the results. Challenges with detecting post-blast residues have led to the use of taggant material as a marker for the explosive [26]; the question of the suitability of such markers in achieving this aim remains open however. Additionally, likely due to the cost of conducting firing trials, the inclusion of repeated firings are limited in previous work. In the limited cases where repeat firings have been possible, variations in the quantity of post-blast explosive residue detected on similar sites following firings of the same explosive charge, configured in the same manner, have demonstrated the unique nature of each detonation event [25].

Using a military and improvised explosive formulation, this study is the first to systematically assess the explosive residue distribution patterns formed following detonations. We incorporate repeated firings and measurement of blast overpressures, environmental conditions and fireball growth in order to test the variables hypothesised to affect explosive particle distribution.

2. Experimental

2.1. Materials

Fertilizer grade ammonium nitrate (AN) prills (Hydro Agri Ltd., UK) were ground to less than 1 mm in diameter using electric processors (average particle size; 0.8 mm). Aluminium powder (10 μm–150 μm average particle diameter, provided by Defence Science and Technology Laboratories, UK) was mixed into the AN in a 10:90 (mass fraction) Al:AN ratio to produce the improvised aluminised AN (AlAN) explosive charges. The military composition used was Plastic Explosive Number 4 (PE4), consisting of 1,3,5-Trinitroperhydro-1,3,5-triazine (RDX) (mass fraction of 88%) as the explosive ingredient and hydroxyl–terminated polybutadiene (HTPB) (mass fraction of ~12%) as the binder (provided by Cranfield Defence Academy). Each explosive was moulded into six spheres of 0.5 ± 0.001 kg mass each in order to conduct repeat firings (approximately 81.79% and 91.89% theoretical mass density for the organic and inorganic charges respectively). SX2 booster charges (88% RDX and 12% non-explosive plasticiser) and No. 8 Instant Electric detonators (containing ~0.7 g of Pentaerythritol tetranitrate) were used to produce detonation.

2.2. Experimental design

All firings were conducted at the Explosive Range and Demonstration Area (ERDA) at Cranfield Defence Academy. Charges were positioned atop wooden firing poles and secured in place with adhesive tape around the base of the charge and top of pole. In order to prevent crater formation, and therefore comply with range operating procedures, each charge was placed 2 m from the ground. New firing poles were used per detonation. Booster charges and detonators were positioned in the charge centres from underneath the charge (detonator tip pointing up) and initiation was therefore directed vertically upward in order to avoid directionally biased expansion of product gases in any of the horizontal orientations.

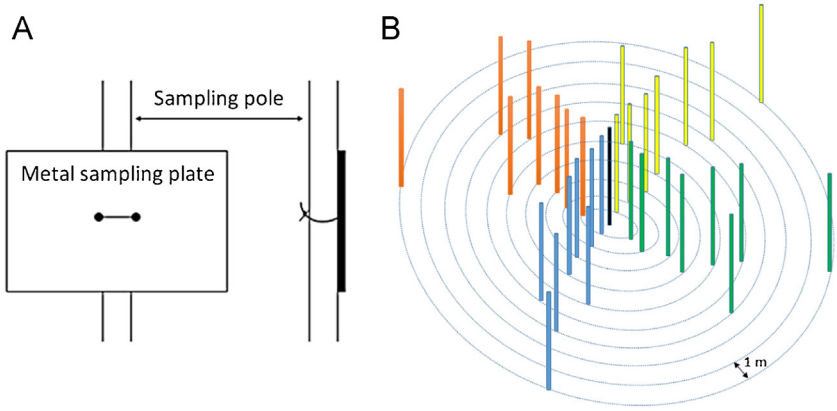

Fig. 1. Experiment set-up, (a) schematic of steel sampling plate attachment on sampling poles, and (b) aerial view of sampling pole positions around centrally positioned explosive charge, at 1 m incremental distances and four orientations around the centre. It was not possible to position sampling poles at 8 m and 9 m due to the terrain on the firing range.

In order to directly capture and sample for post-blast residues, an array of steel 'witness' plates (300 mm × 200 mm × 0.80 mm) was arranged around each charge. Plates were secured 2 m from the ground onto steel 'sampling' poles that were positioned in four orientations around the central firing pole and at 1 m incremental distances from it (Fig. 1). Plates were positioned perpendicular to the ground instead of parallel to it as sampling for explosive residues on surfaces around a blast (that are not on the ground) is more likely to occur on perpendicularly positioned sites such as walls or signposts. The sampling poles were hammered into the ground to secure them in place. All sampling poles were positioned offset with each other (i.e. not directly in front or behind each other) to avoid obstruction of the furthest sampling sites by those closer to the centre.

2.3. Data collection methods

Quartz piezoelectric pressure gauges (Piezotron® type 211B, Kistler, USA) were mounted on 2 m high supports and positioned in the south-east orientation around each charge. The distance of each gauge (1 m, 2 m, 3 m and 4 m) was measured with a laser distance measurer (Leica Disto D210) and each was aligned directly behind the other in order to accurately record the blast wave profile. Data was collected for duration of 20 ms and processed with a 25.0 MHz digital oscilloscope (Nicolet Technologies Sigma 90-8) and based on the waveforms from each firing the peak positive pressures and integrated impulses were calculated.

Each firing was recorded using a high-speed imaging (HSI) camera in order to estimate the fireball and smoke plume volumes produced. A Phantom V12.1 camera (Vision Research, UK) was operated in monochromatic mode at 1280 × 800 full widescreen resolution and 6000 frames per second (fps). The camera was situated 75 m south from the firing area, facing north for each of the firings.

The environmental conditions, including temperature, humidity, barometric pressure, and wind speed and direction were measured and recorded in the centre of the firing area at 2 m from the ground prior to each firing using a Kestrel 3500 weather meter.

Explosive resides were collected using sterile cotton swabs (30 mm diameter, Medline Industries, USA), moistened with 5 cm^3 deionised (DI) water (Sigma Aldrich, UK) for the inorganic explosives and with 5 cm^3 of acetone (>99.8%; Sigma-Aldrich, UK) for the organic explosives; these were used to swab the entire plate surfaces facing the detonations. Each swab was held with disposable sterile polystyrene tweezers (VWR, SA) that were individually packed and opened only prior to sampling. Swabs were applied with pressure horizontally and vertically ensuring the whole plate surfaces were sampled thoroughly and consistently for 30 s each before returning the swabs into 10.5 cm^3 glass squat vials with snap on caps (Scientific Glass Laboratories, UK) containing the original 5 cm^3 of solvent. Vials were labelled with the position of the plate relative to the central firing area and upon returning to the laboratory were refrigerated at ~4 °C. In addition to the test samples obtained after firings, in order to ensure contaminant free equipment and chemicals, swabs of blank (without explosive) plates and blank swabs were extracted for control purposes, as well as blank samples of each solvent used.

2.4. Chemical analysis

Sample vials were sonicated (Grant MXB22 Ultrasonic bath) at 25 °C for 30 min, after which the swabs within were further agitated by pounding with new glass Pasteur pipettes for 2 min in order to further promote the removal of explosive from the swab into the solvent. The extracts were then pipetted into 10 cm^3 disposable polypropylene syringes (Sigma Aldrich, UK) fitted with 0.2 μm pore nylon filters of 30 mm diameter (Chromacol, UK). Each filtrate was then deposited into new, labelled 10.5 cm^3 glass vials.

To the original sample vials, still containing the swab, an additional 5 cm^3 of DI water or acetone was added to the inorganic and organic samples respectively and agitation via sonication and Pasteur pipettes was repeated. This second extract was removed through the swab until dry and filtered into the vials containing filtrate.

A 1.5 cm^3 aliquot of the filtered aqueous samples was pipetted into 1.8 cm^3 chromatography vials (Chromacol, UK) for analysis of NH_4^+ and NO_3^- via ion chromatography (IC). The acetone in the organic filtrate was evaporated and 1.5 cm^3 of HPLC grade acetonitrile (ACN) (99.8%, Sigma Aldrich, UK) was pipetted into each vial to dissolve any RDX residues, to be transferred into chromatography vials for high performance liquid chromatography-mass spectrometry analysis (HPLC–MS).

Operating conditions for the following analyses are detailed in Appendix A of Supplementary material. Analysis of NH_4^+ and NO_3^- was performed using IC on a Dionex ICS-2000 reagent free IC system with eluent generation (Thermo Scientific, USA) coupled to an SRS-300 auto-suppression device and conductivity detector. Samples were analysed for aluminium content using a Varian 720–ES inductively coupled plasma-atomic emission spectrometer (ICP–AES) with an SPS3 autosampler, against matrix matched standards of 1% (volume fraction) nitric acid. HPLC was performed with an Accela capillary LC system (Thermo Scientific, UK) with gradient

micro-pumping system, degasser and thermostated flow manager. RDX was measured in negative electrospray (ESI) mode using the ion trap mass spectrometer. To all samples 0.1% $CHCl_3$ was added in order to form RDX adducts with chlorine (*m/z* 257 observed as [M+Cl]- ions) under negative mode ESI conditions (see Appendix A of Supplementary Information). The quantification of RDX was achieved by using the reconstructed ion chromatogram generated for selected ion monitoring (SIM) set at *m/z* 257 and the area under the peak was calculated as corresponding to the concentration of RDX in the solution injected on the C18 column.

In order to quantify the residues, individual analyte stock solutions (Fisher Chemical, UK) were used to make calibration standards of concentrations ranging between 0.1 and 1000 mg L^{-1}. Calibration lines were constructed by plotting peak area against concentration for each analyte. Linearity was evaluated via the R^2 regression coefficient of determination (all generating R^2 values of over 0.95). Further to the calibrants, quality assurance (QA) standards of each analyte were also produced in order to assess the accuracy of the calibration. Calibration standards were analysed at the beginning, middle and end of each sequence and QA samples analysed at multiple points throughout. All calibrants, QA standards and post-blast test samples were injected in triplicate. Details of the calibration results are presented in Appendix A of Supplementary material.

3. Results and discussion

Values pertaining to the amount of explosive detected are limited by the efficiency of sample collection and instrument sensitivity to target analytes, and are therefore relative to the absolute mass of explosive deposited, which cannot be accurately known. The explosive recovery technique efficiency was evaluated by conducting controlled tests; analyte losses incurred through swabbing, sonication, filtering, and evaporation procedures, resulted in an average recovery of between approximately 25% and 45% of known amounts of RDX and AN deposited onto surfaces respectively, with similar recoveries reported elsewhere [27,28]. Full details and results of the controlled tests are presented in Appendix A of Supplementary material.

3.1. Particle distribution patterns

Initially, the analytes were not found to distribute very strongly according to the theoretical inverse-square law model (red R^2 values inset in Fig. 2), however on exclusion of the datum recovered from 1 m, ammonium, nitrate and RDX corresponded better, generating R^2 values of 0.8562, 0.9958 and 0.9286 respectively (black R^2 values inset in Fig. 2a, b and d). The aluminium distribution did not correlate as well, generating an R^2 of only 0.1907 with the 1 m datum, and of little improvement to a linear fit when this datum was excluded (R^2 0.1959, Fig. 2c).

This is the first time that the distributed explosive residue mass has been shown to correspond approximately to a theoretical model since the inverse-square law was posited to be suitable for understanding particulate dispersal during explosive releases [19]. But these correlations were only improved when the 1 m data was omitted (particularly for the nitrate and RDX), indicating that less residue may deposit at these points due to, for example, blast pressure or fireball temperature effects at such a 'close-in' range. Moreover, this comparison was only significant when established using the total mass of explosive residue detected at each distance (the sum of the four sampled orientations about the centre), which was then averaged over the 6 repeated firings. On examination of the analyte mass, per distance, that was distributed after each firing, the association with the theoretical law became weaker. In fact, only the AN exhibited a noticeably constant decrease in mass as the distance from the detonation increased (Fig. 3a and b) (an anomaly to this being the ammonium trend after firing 3 (Fig. 3a)).

Table 1
Mass range and radii within which the majority of analytes were detected.

Analyte	LOQ[a]	Mass range[b]	Radius[c] (m)
NO_3^-	0.1 mg/L	0 – 14 mg	<10
NH_4^+	0.5 mg/L	0 – 0.3 mg	<10
Al	40 μg/L	0 – 1 μg	<10
RDX	0.1 mg/L	0 – 20 μg	5

[a] limit of quantification.
[b] range of detected amounts of each analyte.
[c] limiting radius around detonation within which residue was detected.

The aluminium distribution was distinctly different, with the greatest amounts detected 5 m from the detonations following the majority of firings (Fig. 3c). The Al had the smallest average particle size range of between ~10 to 80 μm (compared to ~30–1300 μm and ~10–500 μm of AN and PE4 respectively), and this could explain why it dispersed further to be detected in its greatest quantities at 5 m, as different particle sizes have been found to distribute to different distances around a detonation [29]. The ability to discriminate between elemental aluminium particles that remain from the AlAN composition and aluminium from any oxidised products formed during the afterburning process may also be an important criteria in understanding this trend. ICP-AES would not have been able to distinguish between the two however, and moreover, it is likely that any remaining elemental aluminium would be subsequently oxidised in the surrounding atmosphere after deposition onto a sampling plate (i.e. naturally rather than due to afterburning following detonation). Such issues signify that while the aluminium may indeed disperse via a different mechanism to that of the base explosive charge analytes, future tests with an inert material additive would allow further examination of this phenomenon. The variations between Al and AN distributions nonetheless demonstrate that if taggants or additives are to be used as markers for explosives, they must be chemically incorporated into explosive molecules, otherwise it is not necessarily the movement of the explosive that is established.

In contrast, the amount of RDX detected fluctuated with increasing distance, with, in most cases, the greatest mass detected from plates positioned at 2 m (Fig. 3d). Such oscillating trends have been observed for organic post-blast residues previously [30]. This signifies that the application of one theoretical concept to the dispersal of multiple analytes during detonation is unsuitable. The variation between the distribution behaviour of the inorganic and organic analytes could be due to their different detonation behaviours (i.e. how the undetonated particles are ejected from their origin) or variations in the stability of the analytes on closest positioned sampling sites (i.e. the potential thermal degradation of RDX by the fireball), which will be discussed further in Section 3.3.

The wider-spread distribution of the AlAN residues (detected up to 7 m) compared to RDX (majority detected within 5 m) may be explained on a simple mass variation basis; the production of greater quantities of undetonated residual AN from the AlAN charges (up to 50 fold compared to RDX, see Table 1) would distribute over a greater area compared to the RDX. The radii established here correspond well with findings from previous studies that have detected explosive residue between only 2 m and 5 m [31], within 10 m [32,33], and within 15 m [34]; whilst this supports the practice of sampling for explosives near and around the blast centre [19], it also demonstrates that samples can be taken from areas other than the seat or centre of the detonation. As sampling sites could not be placed at 8 or 9 m during these firings, the detection radius for the inorganic analytes could have been further than 7 m, and without this data are therefore stated as <10 m.

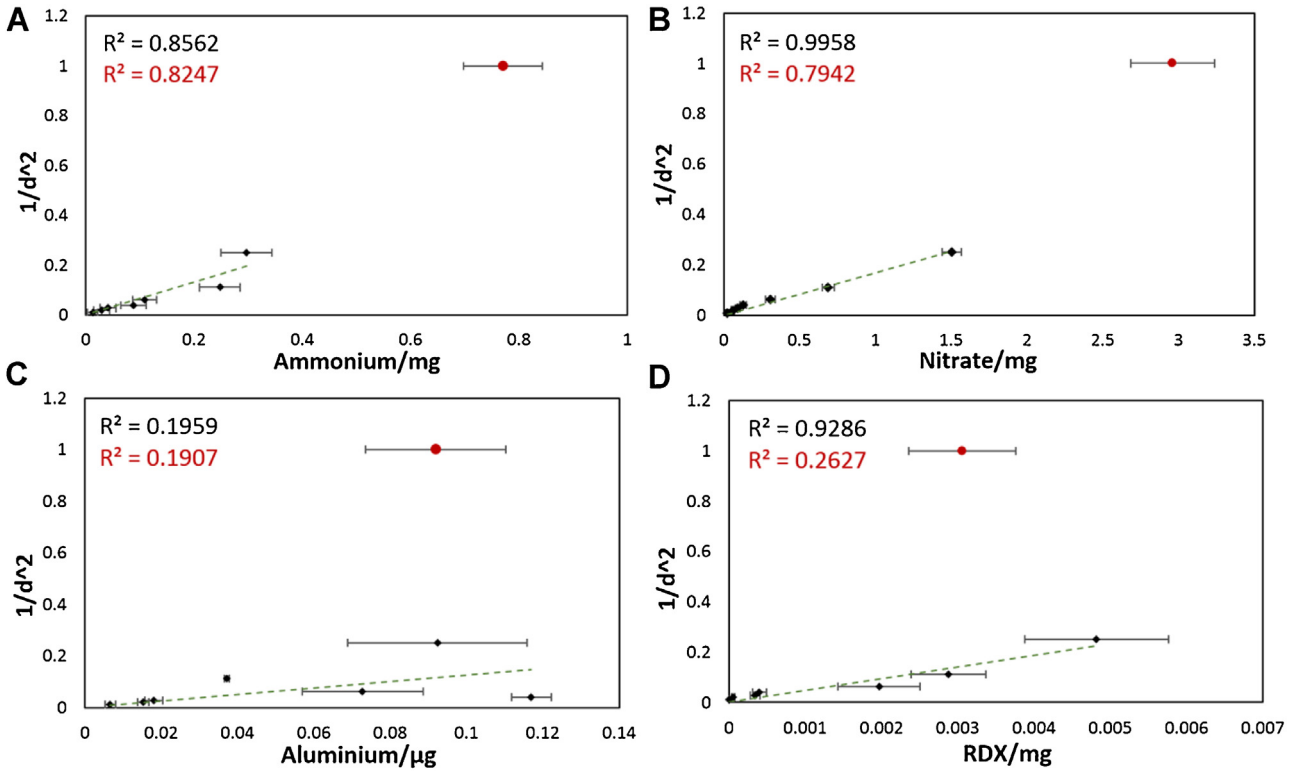

Fig. 2. Total amount of explosive residue detected at each sampled distance compared to '$1/d^{2}$' representing the inverse-square law model, where d is the distance from between 1 and 10 m. Data from the 1 m sampling points is included as a red point and R^2 values for linearity both with the 1 m datum (in red) and without (in black) are inset. Error bars indicate standard deviation of measurements over 6 repeat firings. (For interpretation of the references to colour in this figure legend, the reader is referred to the web version of this article.)

In a post-blast scenario however, for small charges such as these, the application of more sensitive analytical techniques to samples collected further from 7 m from detonations would be required in order to yield beneficial explosive signals.

3.2. Explosive residue mass

The detected mass of Al was comparable between repeated firings (the anomaly being after firing 1, c.f. Fig. 3c), but this was not the case for AN or RDX (Fig. 3a, b and d), which therefore reaffirmed the notion that each detonation event is unique [7,11]. The reproducibility of the trends however, particularly for the inorganic analytes, demonstrates that despite the varying *amounts* of residue detected (which has been found before, [25]), the analytes dispersed in a consistent and reliable pattern.

Additionally, the analytes were detected in different quantities compared to each other. More ammonium nitrate (mg range) was recovered in comparison to RDX (µg range) (Table 1). The higher velocity of detonation (VOD) PE4 (~8440 m/s) [11], having a thinner, faster moving shock-front, would cause a more efficient decomposition of explosive molecules. The slower VOD of the AN based compositions (~5000 m/s) [35] is due to the oxidising component required for combustion not being within the fuel molecule; the resulting wider, slower moving detonation wave through the charge may allow for more undetonated material to remain. Moreover, the greater solubility of inorganic ions (solubility of 0.2 kg AN in 1 m^3 of water at 20 °C) would enhance their detection over that of the organic residue (solubility of 0.008 kg RDX in 1 m^3 of acetone at 25 °C).

The non-stoichiometric relationship between the nitrate and ammonium ions (7:1) was thought to differ from the theoretical molar mass ratio of the two in ammonium nitrate (4:1) due to the suppressed conductivity detector used in IC analysis which would have caused cation suppression [36,37]. The suppressor system was required in order to generate solute specific detection (rather than that including the eluent); the amount of ammonium detected in each sample was therefore likely to be underestimated.

Due to it having a lower initial mass in the original charges (10%), it is unsurprising that the lowest analyte quantities detected were of Al (maximum mass detected ~1 µg); this finding supports other studies that have found the added fuel component to be detected in the lowest concentrations [22–24]. It is important to note however that the filtering step that was necessary prior to chromatographic and spectroscopic analyses could have caused the removal of aluminium and/or Al_2O_3, which would have been insoluble in the water moistened swabs used to collect the inorganic samples. It was not possible to retrieve any particulates trapped within the filter and so this may have caused the seemingly lower concentrations. Nevertheless, aluminium was still detected, and as all of the inorganic samples were treated with the same procedure, it could be assumed that the detected amounts in each samples were relative to the actual deposited amounts (albeit by an unknown ratio); in this case the higher quantities of Al at 5 m from the detonations in the distribution patterns remains unexplained.

Despite potential sampling/extraction issues encountered, fuels are likely to be incorporated as a smaller proportion of an explosive charge and will therefore be less abundant in the post-blast residues. This amplifies the importance of understanding the movement of additives during explosive releases; on suspicion of the use of a chemically, biologically or radiologically modified IED at a post-blast scene, with low, but potentially harmful, amounts of material remaining, it would be necessary to identify areas exposed to such particulates. The finding that the aluminium distributes differently to the main explosive, and that it can be more difficult to detect,

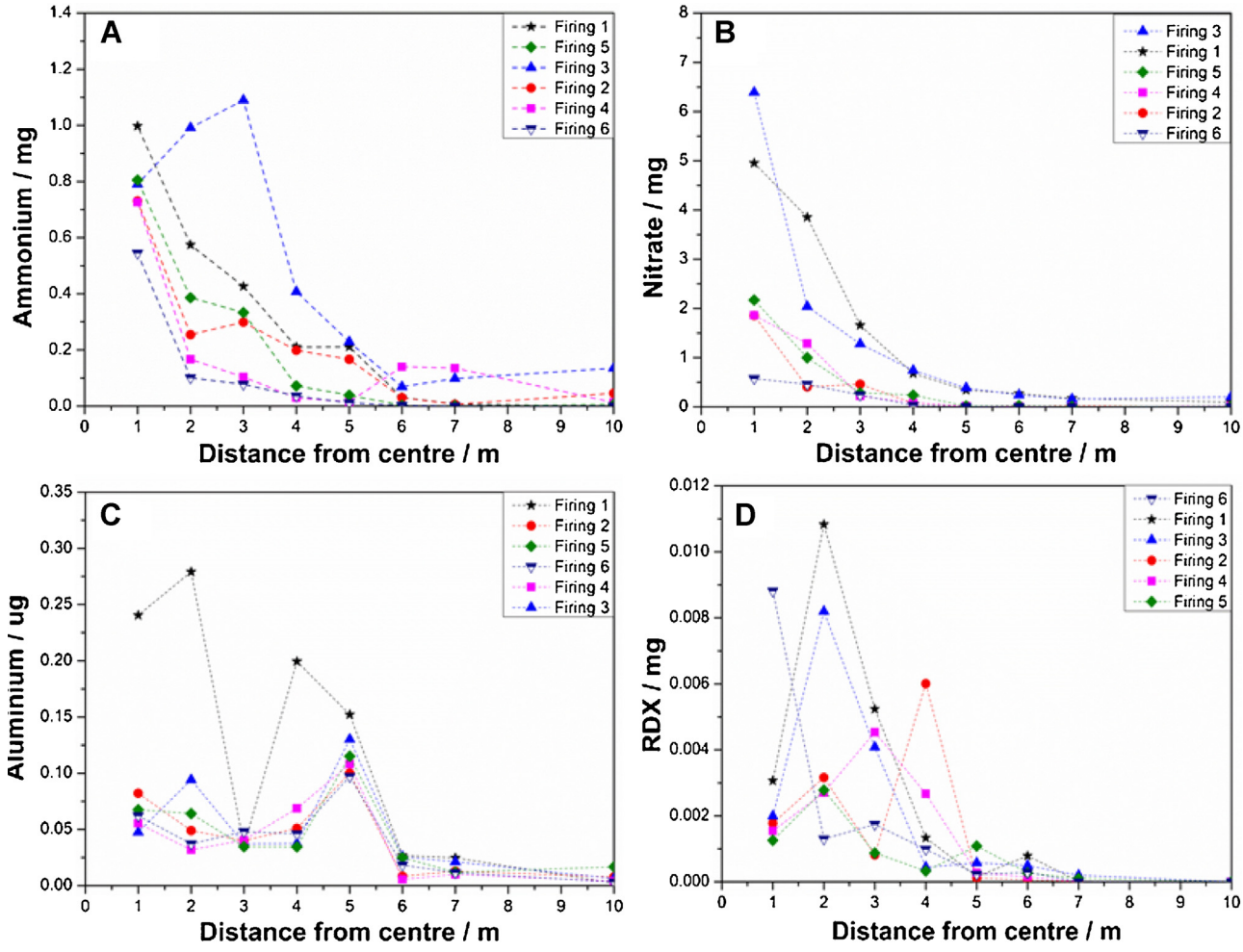

Fig. 3. Explosive residue distributions: mass of analytes detected at each sampled distance around detonations of repeated firings of AlAN (a, b and c) and PE4 (d).

promotes the need to further investigate its dispersal mechanism (and that of other particles that could be potential additives in an explosive charge).

3.3. Dispersal mechanisms

3.3.1. Residue distribution vs. blast wave

Each detonation produced blast-waves consistent with the theoretical Friedlander waveforms [7,11,38] (see Appendix B of Supplementary material). A greater energy release from the PE4 [11] manifested as higher peak overpressures (~479 kPa) compared to the AlAN formulations (~170 kPa).

Hypothetically, undetonated explosive particulates may be ejected away from the bulk charge due to the blast-wave, the positive overpressures of which could cause ejected residues to be pushed outward from the charge surface due to a localised rise in pressure at the charge periphery [18,19,39]. Whilst others [23,24] disagree with this theory, it is currently untested. As spherical charges were used in these experiments, a uniform spherical blast-wave was assumed. If the blast was responsible for particle motion away from the detonation, an inverse-square-like distribution would be expected, as seen with the inorganic analytes, which decreased in concentration between 1 m and 4 m synonymously with the recorded overpressure (Fig. 4a). This would also be expected from the PE4 firings, however, RDX was detected in lower concentrations at 1 m, where blast overpressures were highest, compared to at 2 m where overpressures had decreased (Fig. 4b). It is plausible that initial particle dispersals due to the PE4 blasts may have been affected subsequently by fireball effects, causing lower amounts to be detected at 1 m. Why this would not also occur for the inorganic residues is unknown.

In order to assess the effect of the blast wave further, it would be necessary to use high-speed imaging techniques capable of recording at ultra-fast rates to monitor the movement of boundary layer particles on the charge surface, which is currently challenging to do.

3.3.2. Residue distribution vs. fireball growth

In order to monitor the growth of fireballs and any interactions of the expanding gases with surrounding sampling sites, each detonation was recorded with HSI and representative stills of firings of each composition are presented in Appendix C of Supplementary material. Contrary to the near symmetrical nature of blast-waves from spherical charges [38], fireball dynamics are more sensitive to minor morphological variations [12,40]. The use of a singular angle to record the detonations is reasonable here as it is assumed that considerable variations in estimated fireball radii would not have occurred in unrecorded orientations around the detonations.

Due to instabilities occurring on both a molecular and macro scale [40,41] neither formulation produced completely spherical fireballs. The surfaces of the AlAN fireballs were 'spiky', potentially due to Richtmeyer-Meshkov instabilities occurring at the boundary layer between the fireball and surrounding atmosphere, or due to the protrusion of filamentary jets from the product gases, pro-

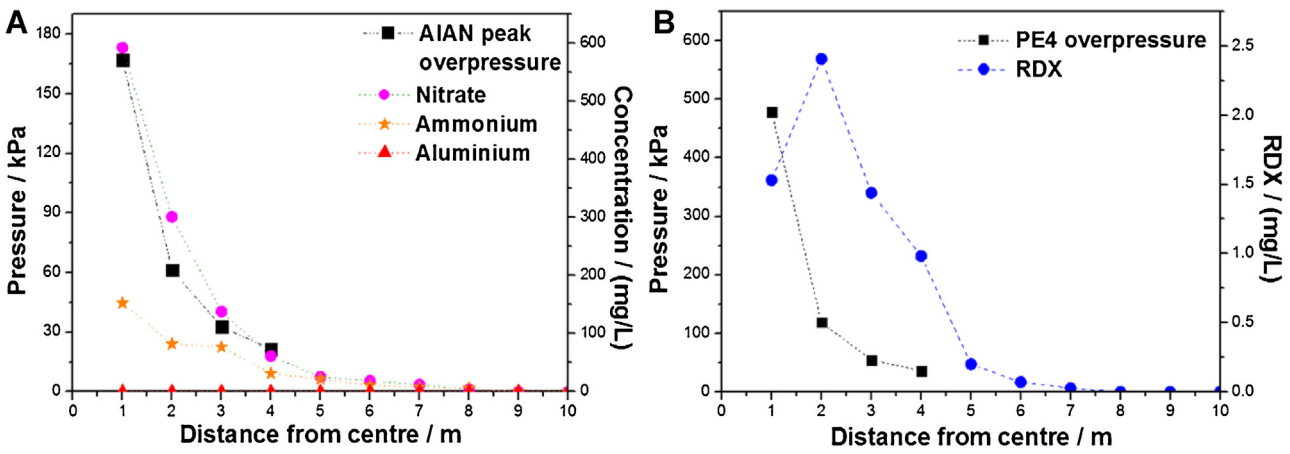

Fig. 4. Blast over-pressure vs. average residue mass distribution for (a) AlAN detonations, and (b) PE4 detonations. The concept of the blast-wave itself carrying or promoting the movement of the particles remains unverified.

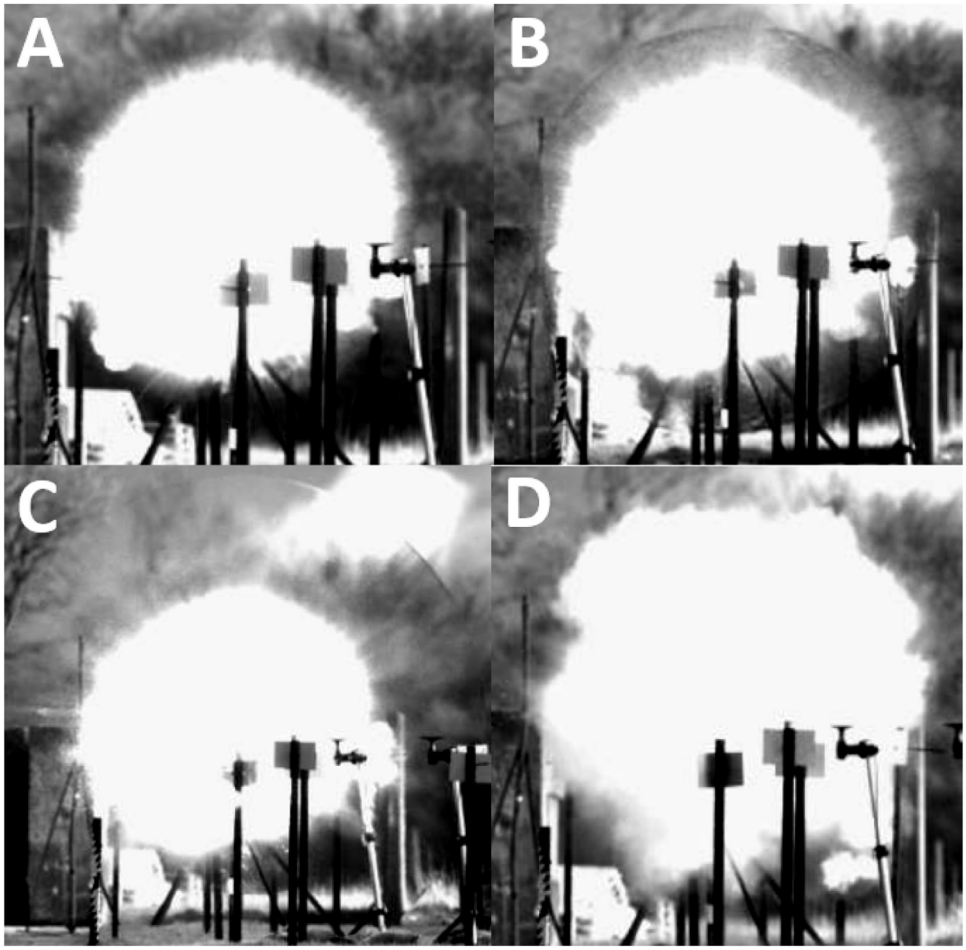

Fig. 5. Representative HSI stills of spherical 0.5 kg AlAN detonation at time (t): (a) t = 1.01 ms, (b) t = 1.67 ms, (c) t = 3.00 ms and (d) t = 23.8 ms.

duced by the aluminium particles upon ignition (Fig. 5a and b) [40]. Closer inspection (i.e. higher magnification and resolution HSI recordings) of the perturbations on the surface of the AlAN fireballs may be able to indicate the cause of such irregularities more definitively. Particulate material was also visible between the blast-wave and fireball surface during the AlAN firings (Fig. 5b), which may be undecomposed explosive moving away from the fireball region to be deposited onto sampling sites, or is more likely the ignition of aluminium particles on reaction with atmospheric oxygen (as this was not observed during the PE4 detonations, Fig. 6b). The observation of these particles within the layer between the blast wave and fireball contradicts the theory that the blast facilitates ejection and movement of particles ahead of it.

As more moles of gas are produced by RDX (Eq. (1)) compared to AN (Eq. (2)), the average size of the PE4 fireballs, observed at their maximum radius, were larger (approx. 2.2 m) compared to those of AlAN (approx. 1.3 m). Any undecomposed explosive adhered to a surface nearby the detonation may be engulfed in the fireball

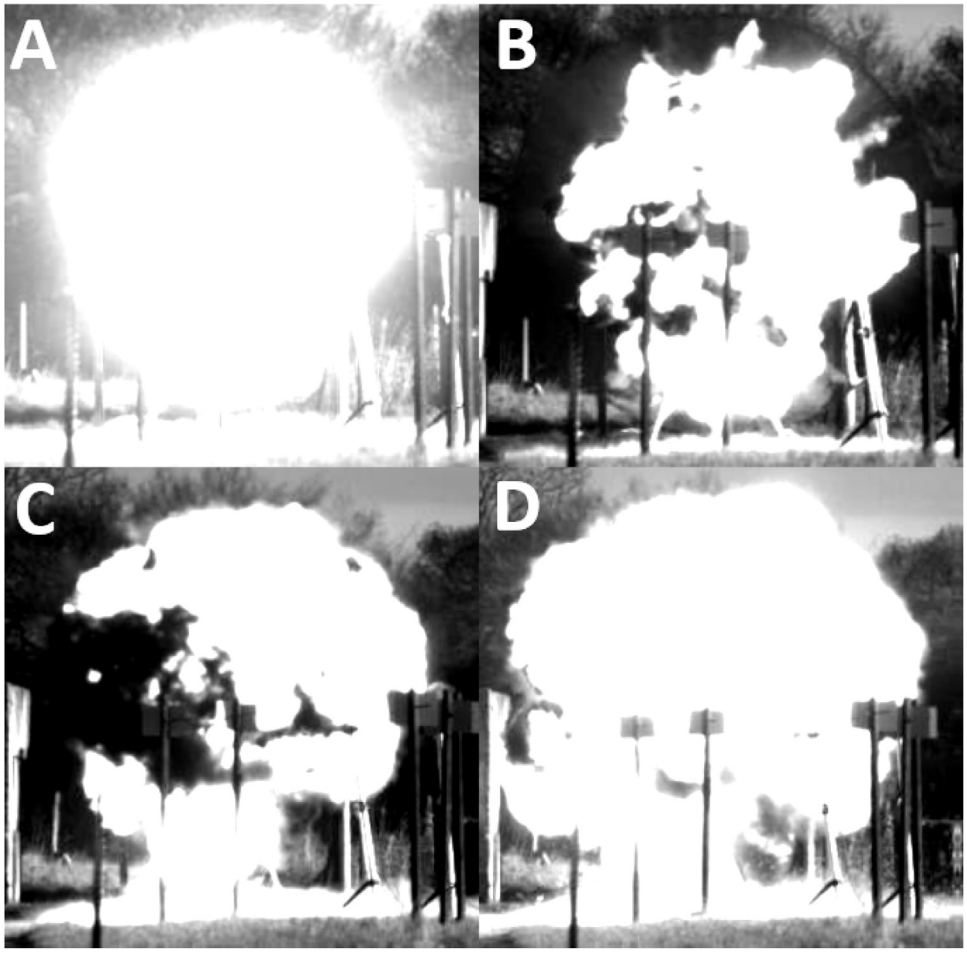

Fig. 6. Representative HSI stills of spherical 0.5 kg PE4 detonation at time (t), (a) t = 0.834 ms, (b) t = 2.17 ms, (c) t = 14.2 ms and (d) t = 37.7 ms.

and decompose on exposure of the flame front (the temperature of which would exceed the thermal decomposition temperature range of the analytes). Using atomic emission spectroscopy, temperatures of ~3000 K have been measured for RDX/HTPB fireballs resulting from detonation (e.g. Ref. [42]), these would be higher than the decomposition temperatures of the resulting post-blast products. The degradation of deposited residues due to the fireball is potentially supported here by the results of the RDX, which was detected in lower quantities within the fireball region (1 m) than at the edge of the fireball region (2 m). The reason for the RDX quantity fluctuations at further distances (4 m to 6 m, c.f. Fig. 3d) from the centre where the fireball was not seen to extend is unknown however.

The addition of combustible metal particles such as Al is known to increase fireball temperatures [43], particularly in the post-blast phase where the products continue to combust. The immediate post-blast temperature of the AlAN detonations would therefore have been at a higher temperature than that of the RDX-based explosives; this makes the finding of greater quantities of ammonium and nitrate at the close by 1 m distances counterintuitive, as these sampling sites were seen to be exposed to the fireball and would have also experienced elevated post-blast temperature. Non-uniform temperatures within the AlAN fireballs may somehow facilitate the persistence of intact AN, which could subsequently be deposited on sampling plates during the smoke plume movement after fireball decay, however the mechanism of how AN could not decompose at such high temperatures is currently uncertain.

The aluminium was detected in greater quantities further from the centre (at 5 m), where the fireball was not observed to extend to (c.f. Fig. 3c). The discrepancy in the aluminium data could be attributed to non-uniform Al afterburning and an assessment of the detonation temperature and immediate post-blast temperature in our future experiments may aid in understanding aluminium combustion around the initial blast.

3.3.3. *Residue distribution vs. environmental conditions*

Environmental conditions, in particular the wind direction, have been posited to affect the particulate dispersal during explosions [18,24,32]; the wind speed during these firings varied between 2.8 m s^{-1} and 5.8 m/s and was consistently in the northward, northwesterly, and westward directions during all firings (Appendix D of Supplementary material contains the recorded data for all environmental parameters). These measurements were recorded immediately prior to each firing; although transient fluctuations would occur in the ambient field, these would not be possible to record during and nearby the detonations. Moreover it is the overall wind direction and velocity that governs the movement of the smoke plume and it was therefore assumed that over the time period of significant interest here (millisecond scale), the wind was a steady flow.

The amount of residue detected on sample sites positioned at equal distances from the detonations, but in different orientations about the centre, was dissimilar. This directional bias was due to the wind direction at the time of firing as the majority of the greatest quantities of analytes were recovered from sampling sites posi-

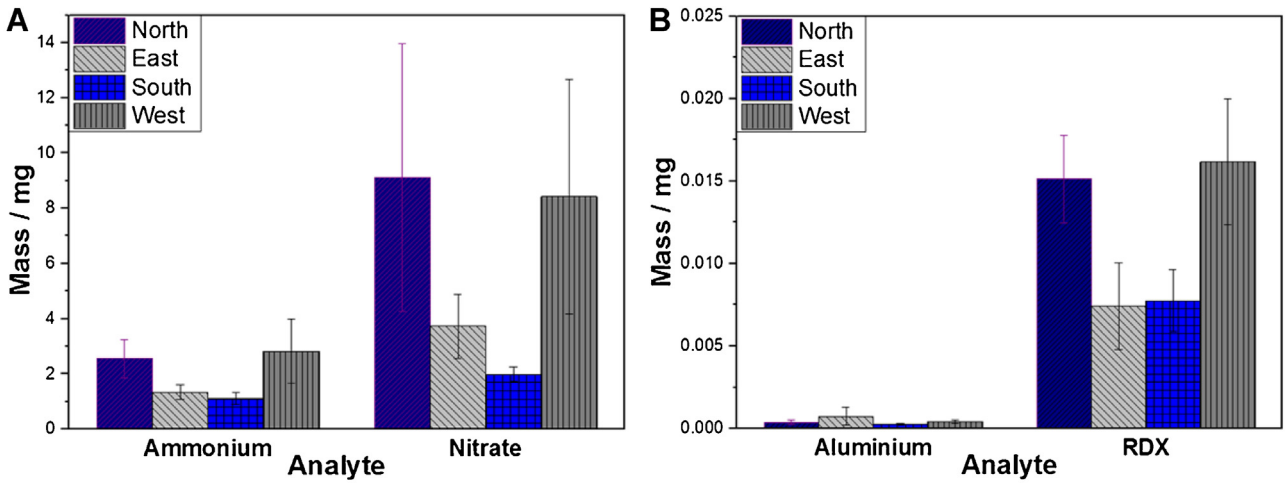

Fig. 7. Residue distributions per sampled orientation around the charge centres for (a) ammonium and nitrate, (b) aluminium and RDX.

tioned downwind (and the smoke plume had therefore moved passed). Ammonium nitrate and RDX distributions were skewed with the wind direction in most cases (Fig. 7), indicating that the movement of undetonated residues was occurring in the smoke plume, which would be governed by the wind field. The trend was less obvious for the aluminium though (Fig. 7b), which whilst detected in the lowest amounts from upwind sites (south-facing) was detected in the greatest quantities from eastward sites that were not in line with the wind direction. This is again suggestive of additive material having a different dispersal mechanism and potentially impacts on the way in which other additives may move.

The means by which undetonated explosive particles can remain within the smoke plume is unknown; the unreacted material could persist somehow in the fireball, the temperature of which would not be uniform throughout and regions of 'lower' temperature, relative to the fireball centre for example, could potentially facilitate the survival of intact explosive. Conversely, non-uniformities in the charge configuration may lead to ejection of material that is subsequently affected by the wind prior to completion of detonation. Though the exact mechanisms posited here for undetonated residue persistence remain speculative, it is clear that there is a correlation between the depositions of most analytes with the wind direction. In order to fully test the true effect of the wind it would be necessary to conduct an experiment when there is no dominant wind field, or where an externally forced one-directional flow can be applied, however such a 'controlled' test would not be possible during outdoor firings. In an ideal scenario, the use of an indoor firing chamber would be an appropriate method of controlling the environmental conditions during firing; such a chamber would need to be large enough so that significant blast reflections from walls were not encountered in areas of sampling, and it would need to be free from explosive residue contamination from any previous firings.

4. Conclusions

Mathematical models can be applied to understanding general particle distribution patterns during detonation, however, actual trends are analyte specific. The distribution of AN is thought to occur as multi-phase process, initially spalled from the charge surface, potentially caused by blast-wave effects, particles can consequently disperse approximately according to an inverse-square law model. Subsequently, any residual undetonated material amongst the gaseous products is dispersed in the smoke plume by the wind. The PE4 distributions were more random; thermal degradation of closely deposited undetonated particles due to the fireball expansion is likely, with the wind field again being the more robust dispersal mechanism. Aluminium, added to the AN, was the only analyte that was consistently detected in greater quantities further from the detonations, indicating the dispersal mechanism of additives is different to that of the base-explosive analytes.

The findings here support forensic practices of sampling for explosive residues around the central detonation region (not necessarily at the explosion seat or centre), but also highlight further important criteria that should be considered, including the use of CCTV if available, to establish the movement of the smoke cloud and thereby determine potential residue deposition sites at further distances from the detonation centre, up to 10 m away even. This current study also stimulates new, important questions such as how can undetonated explosive remain within product gas expansion in the first instance? And, why does the movement of additives vary to that of the base explosive analytes, and how does this change when the complexity of the system is increased (i.e. using non-spherical, confined charges positioned near structures)? Development of such a particle dispersion knowledge base would benefit sampling procedures for forensic, public health and environmental decontamination purposes in the post-blast domain.

Acknowledgements

This study was supported by the UK EPSRC (Grant EP/G037264/1). Jim Clements, Graeme Creighton and Paul Walker are thanked for help on the firing range. Three anonymous reviewers are thanked for their comments and advice, which improved the manuscript.

Appendix A. Supplementary data

Supplementary data associated with this article can be found, in the online version, at http://dx.doi.org/10.1016/j.jhazmat.2016.04.081.

References

[1] P. Mostak, Vapour and trace detection of explosives, in: M. Krausa, A.A. Reznev (Eds.), Vapour and Trace Detection of Explosives for Anti-terrorism Purposes, Kluwer Academic Publishers, Netherlands, 2004, pp. 23–31.
[2] P.D. Zimmerman, C. Loeb, Dirty bombs: the threat revisited, Defense Horizons 38 (2004) 1.
[3] Committee on Identifying the Needs of the Forensic Sciences Community, National Research Council, Strengthening Forensic Science in the United

States: A Path Forward, Report No. 228091, The National Academies Press, 2009.
[4] T.R. Botcher, C.A. Wight, Explosive thermal decomposition mechanism of RDX, J. Phys. Chem. 98 (1994) 5441–5444.
[5] D. Chakraborty, R.P. Muller, S. Dasgupta, W.A. Goddard, The mechanism for unimolecular decomposition of RDX (1 3,5-Trinitro-1,3,5-triazine), an ab initio study, J. Phys. Chem. A 104 (2000) 2261–2272.
[6] C.J. Wu, L.E. Fried, First principles study of high explosive decomposition energetics, in: Proceedings of the 11th International Symposium on Detonation, August 31–September 4, Snowmass Village, Colorado, 1998.
[7] J. Akhavan, The Chemistry of Explosives, 3rd ed., Royal Society of Chemistry, Cambridge, 2004.
[8] K.C. Gross, Phenomenological Model for Infrared Emissions from High Explosive Detonation Fireballs, PhD Thesis, Department of the Air Force Air University, Air Force Institute of Technology, Ohio, 2007.
[9] S. Chaturvedia, P.N. Davea, Review on thermal decomposition of ammonium nitrate, J. Energ. Mater. 31 (2013) 1–26.
[10] F.J. Owens, J. Sharma, X-ray photoelectron spectroscopy and paramagnetic resonance evidence for shock-Induced intramolecular bond Breaking in some energetic solids, J. Appl. Phys. 51 (1980) 1494–1497.
[11] G.F. Kinney, K.J. Graham, Explosive Shocks in Air, Springer-Verlag, New York, 1985.
[12] K. Balakrishnan, S. Menon, On the role of ambient reactive particles in the mixing and afterburn behind explosive blast waves, Combust. Sci. Technol. 182 (2010) 186–214.
[13] C.K. Kim, J.G. Moon, J.S. Hwang, M.C. Lai, K.S. Im, Afterburning of TNT explosive products in air with aluminum particles, in: 46th AIAA Aerospace Sciences Meeting and Exhibit, 7–10 January, Reno, Nevada, 2008.
[14] M.H. Keshavarz, A simple theoretical prediction of detonation velocities of non-ideal explosives only from elemental composition, in: P.B. Warey (Ed.), New Research on Hazardous Materials, Nova Science Publishers, USA, 2006, pp. 255–25737.
[15] A. Maranda, Research on the process of detonation of explosive mixtures of the oxidizer fuel type containing aluminium powder, Propellants Explos. Pyrotech. 15 (1990) 161–165.
[16] J. Paszula, W.A. Trzciński, K. Sprzatczak, Detonation performance of aluminium −Ammonium nitrate explosives, Center Eur. J. Enery Mater. 5 (2008) 3–11.
[17] W.A. Trzciński, S. Cudziło, J. Paszula, Studies of free field and confined explosions of aluminium enriched RDX compositions, Propellants Explos. Pyrotech. 32 (2007) 502–508.
[18] N. Abdul-Karim, C.S. Blackman, P.P. Gill, E.M.M. Wingstedt, B. A. P. Reif B. A. P., Post-blast explosive residue −a review of formation and dispersion theories and experimental research, RSC Adv. 4 (2014) 54325.
[19] H.J. Yallop, Explosion Investigation, Forensic Science Society and Scottish Academic Press Ltd, Edinburgh, 1980, pp. 21–89.
[20] N. Abdul-Karim, R. Morgan, R. Binions, T. Temple, K. Harrison, Spatial distribution of post-Blast RDX residue: forensic implications, J. Forensic Sci. 58 (2012) 365–371.
[21] J. C. Pennington, T. F. Jenkins, G. Ampleman, S. Thiboutot, J. M. Brannon, A. D. Hewitt, J. Lewis, S. Brochu, E. Diaz, M. R. Walsh, M. E. Walsh, S. Taylor, J. C. Lynch, J. Clausen, T. A. Ranney, T. A. Ramsey, C.A. Hayes, C. L. Grant, C. M. Collins, S. R. Bigl, S. Yost, S. K. Dontsova, Distribution and Fate of Energetics on DoD Test and Training Ranges: Final Report, Engineer Research and Development Center, 2006.
[22] S. Phillips, A. Lowe, M. Marshall, P. Hubbard, S.G. Burmeister, D.R. Williams, Physical and chemical evidence remaining after the explosion of large improvised bombs. part 1: firings of ammonium nitrate/sugar and urea nitrate, J. Forensic Sci. 45 (2000) 324–332.
[23] H. Cullum, A. Lowe, M. Marshall, P. Hubbard, Physical and chemical evidence remaining after the explosion of large improvised bombs. part 2: firings of calcium ammonium Nitrate/Sugar mixtures, J. Forensic Sci. 45 (2000) 333–348.
[24] A.M. Monsfield, M. Marshall, C.L. Walker, P. Hubbard, Physical and chemical evidence remaining after the explosion of large improvised bombs. part 3: firings of calcium carbonate ammonium Nitrate/Sugar, J. Forensic Sci. 46 (2001) 535–548.
[25] R. Borusiewicz, G. Zadora, J. Zieba-Palus, Chemical analysis of post explosion samples obtained as a result of model field experiments, Talanta 116 (2013) 630–636.
[26] T. Kirkendall, J. Baker, J. H. Barnes, C. Lewis, M. Wheeler, Lanthanide Taggants for Characterizing the Explosive Blast Radius of Homemade Explosive Mixtures, in Pittcon, Philadelphia, USA, 2013.
[27] R.Q. Thompson, D.D. Fetterolf, R.F.M. Miller, Aqueous recovery from cotton swabs of organic explosives residue followed by solid phase extraction, J. Forensic Sci. 44 (1999) 795–804.
[28] J.B.F. Lloyd, R.M. King, One pot processing of swabs for organic explosives and firearms residue trace, J. Forensic Sci 35 (1990) 956–959.
[29] N. Abdul-Karim, C. Blackman, P.P. Gill, R.M. Morgan, L. Matjacic, R. Webb, W.H. Ng, Morphological variations of explosive residue particles and implications for understanding detonation mechanisms, Anal. Chem. 88 (2016) 3899–3908.
[30] P. Ulbrich, R. Varga, Some experience with trace analysis of post-Explosion residues, Acad. Appl. Res. Milit. Sci. 3 (2004) 633–646.
[31] P. Kolla, A. Sprunkel, Identification of dynamite explosives in post explosion residues, J. Forensic Sci. 40 (1995) 406–411.
[32] M. E. Walsh, C. M. Collins, C. H. Racine, T. F. Jenkins, A. B. Gelvin, T. A. Ranney, Sampling for Explosives Residues at Fort Greely, Alaska: Reconnaissance Visit July 2000, US Army Corps of Engineers, Cold Regions Research and Engineering Laboratory Technical Report TR-01-15, 2001.
[33] T. F. Jenkins, T. A. Ranney, P. H. Miyares, N. H. Collins, A. D. Hewitt, Use of Surface Snow Sampling to Estimate the Quantity of Explosive Residues Resulting from Landmine Detonations, US Army Corps of Engineers ERDC/CREEL Report No. TR-00-12, 2000.
[34] J.C. Pennington, C.A. Hayes, S. Yost, T.A. Crutcher, T.A. Berry, J.U. Clarke, M.J. Bishop, Explosive residues from blow in place detonations of artillery munitions, Soil Sediment Contam. Int. J. 17 (2008) 163–180.
[35] A.C. Van der Steen, H.H. Kodde, A. Miyake, Detonation velocities of the non-Ideal explosive ammonium nitrate, Propellants Explos. Pyrotech. 15 (1990) 58–61.
[36] C. Johns, R.A. Shellie, O.G. Potter, J.W. O'Reilly, J.P. Hutchinson, R.M. Guijt, Identification of homemade inorganic explosives by ion chromatographic analysis of post-blast residues, J. Chromatogr. A 1182 (2008) 205–214.
[37] J. Weiss, Conductivity detection in cation chromatography—pros and cons of suppression, Dionex Environ. Rep. (2011).
[38] H.L. Brode, Blast wave from a spherical charge, Phys. Fluids 2 (1959) 217–229.
[39] J.D. Kelleher, Explosives residue: origin and distribution, Forensic Sci. Commun. 4 (2002) (Issued online by US Federal Bureau of Investigation).
[40] D.L. Frost, Z. Zarei, F. Zhang, Instability of combustion products interface from detonation of heterogeneous explosives, in: Proceedings of 20th International Colloquium on the Dynamics of Explosion and Reaction Systems, July 31–August 5, Montreal, Canada, 2005.
[41] L.A. Kuhl, J.B. Bell, V.E. Beckner, K. Balakrishnan, A.J. Aspden, Spherical combustion clouds in explosions, Shock Waves 23 (2013) 233–249.
[42] W.K. Lewis, C.G. Rumchik, Measurement of apparent temperature in post-Detonation fireballs using atomic emission spectroscopy, J. Appl. Phys. 105 (2009) 1–4.
[43] S. Goroshin, D.L. Frost, J. Levine, A. Yoshinaka, F. Zhang, Optical pyrometry of fireballs of metalized explosives, Propellants explos. Pyrotech. 31 (2006) 169–181.